Initial Spread of ^{137}Cs from the Fukushima Dai-ichi Nuclear Power Plant over the Japan Continental Shelf: A Study Using a High-resolution Global-Coastal Nested Ocean Model

Zhigang Lai[1, 2], Changsheng Chen[2,7], Robert Beardsley[3], Huichan Lin[2,7], Rubao Ji[4,7], Jun Sasaki[5] and Jian Lin[6]

[1]School of Marine Sciences
Sun Yat-Sen University
Guangzhou, China

[2]School for Marine Science and Technology
University of Massachusetts-Dartmouth
New Bedford, MA 02744, USA

[3]Department of Physical Oceanography
Woods Hole Oceanographic Institution
Woods Hole, MA 02543, USA

[4]Biology Department
Woods Hole Oceanographic Institution
Woods Hole, MA 02543, USA

[5]Department of Socio-Cultural Environmental Studies
Graduate School of Frontier Sciences
The University of Tokyo
Kashiwanoha, Kashiwa 277-8563, Japan

[6]Department of Geology & Geophysics
Woods Hole Oceanographic Institution
Woods Hole, MA 02543, USA

[7]International Center for Marine Studies
Shanghai Ocean University, Shanghai, 201306, P. R. China

Corresponding Author: Zhigang Lai
Email: laizhig@mail.sysu.edu.cn
Phone: 01-86-13316007200

Abstract

The March 11, 2011 Tōhoku M9 and M7.9 earthquake-induced tsunami destroyed facilities at the Fukushima Dai-ichi Nuclear Power Plant (FNPP) that led to a significant long-term flow of the radionuclide ^{137}Cs into coastal waters. A high-resolution global-coastal nested ocean model was first constructed to simulate the March 11 tsunami and coastal inundation. Based on the model's success in reproducing the observed tsunami and coastal inundation, model experiments were then conducted with differing resolution to assess the initial spread of ^{137}Cs over the east shelf of Japan. The ^{137}Cs was tracked as a conservative tracer in the three-dimensional model flow field over the period March 26-August 31, 2011. The results clearly show that for the same ^{137}Cs discharge, the model-predicted spreading of ^{137}Cs was sensitive not only to model resolution but also the FNPP seawall structure. A coarse-resolution (~2 km) model simulation led to an overestimation of lateral diffusion and thus faster dispersion of ^{137}Cs from the coast to the deep ocean, while advective processes played a more significant role when the model resolution at and around the FNPP was refined to ~ 5 m. By resolving the pathways from the leaking source to the southern and northern discharge canals, the high-resolution model better predicted the ^{137}Cs spreading in the inner shelf where in situ measurements were made 30 km off the coast. The overestimation of ^{137}Cs concentration near the coast is thought to be due to the omission of sedimentation processes in the model, which was evident in sediment measurements taken after the accident.

1 Introduction

The March 11, 2011 Tōhoku magnitude 9.0 and 7.9 earthquakes caused a massive tsunami with ~16-m wave height nearshore and tsunami-induced inundation that devastated the east coast of Japan (Fig. 1). Unlike previous earthquake-induced tsunami events, the Fukushima Dai-ichi Nuclear Power Plant (FNPP) was seriously damaged, resulting in leaking of large amounts of artificial radionuclides, mainly ^{131}I ($t_{1/2}$ = 8.02 days), ^{134}Cs ($t_{1/2}$ = 2.065 years) and ^{137}Cs ($t_{1/2}$ = 30.17 years), from several reactor units into the coastal ocean (Ohnishi, 2012). In this event, the planned dumping from the storage room contained low-level radioactive water, while the leaking from reactors contained high-level radioactive water, with a concentration of 9.4×10^{14} Bq for ^{137}Cs and ^{134}Cs as well as 2.8×10^{15} Bq for ^{131}I from Unit-2 over the period April 1-6 and of 9.8×10^{12} Bq for ^{137}Cs, 9.3×10^{12} Bq for ^{134}Cs, and 9.5×10^{12} Bq for ^{131}I from Unit-3 over the period May 10-11. In comparison to the Chernobyl disaster in 1986, this was not the most serious radionuclide-release in the past. But, the Chernobyl Nuclear Power Plant was located inland and its impact on the Black and Baltic Seas was through deposition with a value of 10^5 Bq, smaller than what happened at the FNPP. As a result, following the March 11 2011 tsunami event, in addition to the wet and dry deposition from the atmosphere, the coastal water was contaminated by discharges of a large portion of high-level radioactive water out of FNPP from leaking sources (Honda et al., 2012) and from inland-polluted rivers (Oura and Ebihara, 2012).

Among these radioactive isotopes, ^{137}Cs was of particular interest because of its long 30.2 year half-life. The accumulation of ^{137}Cs in marine food chains could exert a profound impact on marine biota and human health and thus the local to regional ecosystem (Buesseler et al. 2011; Grossman, 2011). Determining accurately an initial dispersion of ^{137}Cs off Japan's coast was a prerequisite for assessing its long-term impacts on the interior Pacific Ocean. After leaking occurred, many efforts were made on monitoring the spread of ^{137}Cs off Japan's coast. Ministry of Education, Culture, Sport, Sciences and Technology (MEXT) (http://radioactivity.nsr.go.jp/ja/list/238/list-1.html) and Tokyo Electric Power Company (TEPCO) (http://radioactivity.nsr.go.jp/ja/list/239/list-1.html) started measuring the ^{137}Cs concentration around the FNPP and in the offshore coastal waters (Figs 2 and Fig. 3). In addition to these two government-established monitoring programs, several field surveys were carried out in an offshore region to assess the spreading of ^{137}Cs by oceanic currents, lateral diffusion and vertical mixing (e.g., Honda et al., 2012; Behrens et al., 2012; Dietze and Kriest, 2012). The research team led by K. Buesseler (Woods Hole Oceanographic Institution) made a comprehensive survey in the shelf and deeper waters off FNPP in June 2011. Their survey measured ^{137}Cs concentration over the inner-shelf area 30 km away from the coast and then along several transects across the Kuroshio in the deep ocean (Fig. 3). The data collected from these monitoring and field surveys have provided a direct assessment of temporal change and spatial distribution of ^{137}Cs concentration in the coastal waters. Due to the complex nature of advection and mixing in this coastal region, however, these data cannot alone be used to predict the spreading processes of ^{137}Cs from FNPP in the shelf waters after the leaking started. This is one of the key reasons why an ocean model was proposed for this purpose.

It is not a trivial task for a model to simulate and predict accurately the spatial distribution and temporal change of the ^{137}Cs concentration off the Japan coast. Since advection and mixing are two key physical processes that control the spread of ^{137}Cs in ocean waters, we need an ocean model that is capable of resolving an integrated coastal and regional circulation system over scales from a few meters (small scale, e.g. around FNPP) to a few kilometers (mesoscale) over the shelf. The flow around FNPP and near the coast is mainly controlled by tidal exchange, winds and local geometry. The circulation in this shelf region includes the Kuroshio on the south, the Oyashio Current on the north, Tsugaru Current from Tsugaru Strait, and multiple eddies formed in the intersection area of these currents (Fig. 1). To simulate the outflow from FNPP, we need a model with accurate fitting of complex coastal geometry within and around FNPP. The water over the shelf was always stratified so that water temperature and salinity must be included in the model simulation. Several regional-scale ocean model exercises have been made to simulate the ^{137}Cs spread from FNPP, e.g., Kawamura et al. (2011) and Tsumune et al. (2012) with a spatial resolution of 2 km or larger, and Estournel et al (2012) with a resolution of 0.6 km. However, the water exchange between FNPP and the surrounding ocean is through a ~200-m wide narrow entrance between the two breakwaters. The FNPP seawall structure between the two discharging canals (namely, the north and south discharging canals) is ~1300 m. Without sufficient model resolution to accurately capture the complex pathways of ^{137}Cs from FNPP, assessments made by these regional-scale models could be biased with large uncertainty. It is not clear, however, to what degree this bias could be. Could the bias caused by model resolution and geometric fitting issues led to a significant different conclusion about the dispersion of ^{137}Cs off the Japan coast or reproduce the same distribution with just a small difference in accuracy? To our knowledge, this issue has not been well addressed yet in previous modeling experiments.

Geometric fitting of complex coastlines around FNPP and in coastal regions is a critical factor to resolve multi-scale geometrically-controlled near-shore advection while sufficient model resolution is prerequisite of capturing a realistic lateral dispersion. Chen et al. (2008) conducted a model-dye comparison experiment over Georges Bank, with an aim of examining the impact of model resolution on lateral dispersion in the coastal ocean. They found that in order to simulate accurately the observed lateral dispersion within a tidal mixing front with a spatial variation scale of a few kilometers, model resolution down to ~500 m or less was required. Overestimation of lateral dispersion due to model resolution varied in space and time, which could be 4-10 times larger as the model grid size is bigger than 2-4 km. As a result, the model could point to an unrealistic conclusion that differed significantly from the dye observations. The dynamical processes off the FNPP coast are more complicated than on Georges Bank, so that failure to adequately resolve the important spatial scales in this region might lead to a large lateral dispersion rate and thus overestimate the offshore spreading of ^{137}Cs over the eastern Japan shelf.

The biggest challenge for a model to provide an accurate simulation of the spatial distribution and temporal change of ^{137}Cs over the Japan shelf is the large uncertainty in the estimation of the total amount of ^{137}Cs leaking into the water. The leaking lasted for months, so that the source was both spatially- and time-dependent (Estournel et al, 2012). One approach to solve this problem is to treat ^{137}Cs as a conservative tracer and inversely determine its source amount by tracking it in the flow field for a relatively short period during which the model-predicted tracer field had the best match to observations. This method was used to evaluate the total amount of ^{137}Cs from FNPP in the previous modeling experiments made by Kawamura et al. (2011), Tsumune et al. (2012), and Estournel et al. (2012). This method is generally sound, but an adjustment in this type of inverse tracking could vary from model to model, particularly for the case with different model resolutions and setups. Due to this uncertainty, the more interesting model problem, to our opinion, is on gaining knowledge of the sensitivity of the model assessment results to model skill and configuration rather than on evaluating how well a model simulates the observed ^{137}Cs concentration.

We, an international research team with members from the University of Massachusetts-Dartmouth, Woods Hole Oceanographic Institution and Yokohama National University, have developed a high-resolution global-regional-coastal integrated seismic-ocean-tracer FVCOM model system to simulate the March 11 earthquake-induced tsunami, coastal inundation and initial spread of ^{137}Cs. Taking advantage of the geometric flexibility of the unstructured triangular grid, the model has a local resolution of up to 5 m around FNPP and near the coast. Nesting with the global-FVCOM hindcast field with data assimilation of satellite-derived sea surface temperature and sea surface height, the high-resolution regional-coastal FVCOM model not only resolved a realistic regional circulation but also provided a better representation of the water exchange between FNPP and the surrounding ocean. Built on our success in simulating the observed tsunami and coastal inundation (Chen et al., in revision), we applied this model system to track ^{137}Cs over the period March 26 - August 31, 2011. Our studies were aimed at assessing the impact of multi-scale physical processes on the initial spread of

^{137}Cs in the coastal region of Japan. The results were presented in several conferences (Beardsley et al., 2012, Lai et al., 2012, Chen et al., 2012) and many invited talks. A detailed description and summary of model results are given here.

2 The model and design of numerical experiments

The ^{137}Cs was tracked as a conservative tracer in the three-dimensional (3D) flow field predicted by the high-resolution nested global-coastal FVCOM model over the period March 26-August 31, 2011 (Fig. 4). Hereafter we refer to the global FVCOM model as Global-FVCOM and the Japan coastal FVCOM model as JC-FVCOM. FVCOM is the prognostic, unstructured-grid Finite-Volume Community Ocean Model originally developed by Chen et al. (2003) and upgraded by the FVCOM team (Chen et al., 2006a-b, 2012). FVCOM solves the flux form of the governing equations in control volumes constructed with multi-triangular meshes using a second-order accurate discrete flux scheme, which provides accurate fitting of irregular coastal geometries and flexibility in adjusting the grid resolution to capture the key physical processes (Chen et al., 2007). The finite-volume approach ensures local mass, heat, salt, and tracer conservation in the sense of numerical computation, which is suitable to trace ^{137}Cs for this study. The tracer module of FVCOM was validated through a model-dye comparison experiment made on Georges Bank in the northern North Atlantic Ocean by Chen et al. (2008).

Global-FVCOM is a fully ocean-ice coupled model covering the entire global ocean with a grid resolution of ~2 km along the eastern Japanese coast (Fig. 4). The vertical grid discretization was implemented using a hybrid terrain-following coordinate with a total of 45 layers (Chen et al., in revision). The *s*-coordinate was used in regions with depth greater than 225 m, in which 10 and 5 uniform layers with a thickness of 5 m were specified near the surface and bottom, respectively. The uniform thickness σ-coordinate was employed in regions of depth less than 225 m. The coordinate transition occurred at the depth of 225 m where all layers have a uniform thickness of 5 m. Global FVCOM was driven by astronomical tidal forcing with eight constituents (M_2, S_2, N_2, K_2, K_1, O_1, P_1 , and Q_1) and the NCEP reanalysis meteorological forcing fields (surface wind stress, net heat flux/shortwave irradiation, air pressure gradients, precipitation minus evaporation (*P*-*E*), and freshwater discharge from all major rivers along the coast. Initialized with the assimilated model fields at the end of December 31, 2010, we ran Global-FVCOM for the period January 1, 2011 - August 31, 2011 for this ^{137}Cs tracking experiment. To ensure that Global-FVCOM was capable of capturing the regional circulation along the eastern Japanese coast, satellite-derived sea surface temperature (SST) (http://www.nodc.noaa.gov/SatelliteData/ghrsst) and AVISO sea surface height (SSH) (http://www.aviso.oceanobs.com/en/data/products/sea-surface-height-products.html) were assimilated into the model. Global-FVCOM has been validated through a 50-year spin-up simulation and a 33-year (1978-2010) hindcast assimilation (Gao, 2011; Hu et al., 2011)

JC-FVCOM was configured with horizontal resolution varying from 2 km near the boundary nesting with Global-FVCOM to 5-10 m in the nearshore coastal region (including the FNPP) (Fig. 4). JC-FVCOM had the same hybrid vertical coordinate system with 45 layers and was forced with the same meteorological forcing as Global-FVCOM.

To assess the importance of resolving the detailed geometry around the leaking facility on the temporal and spatial distribution of ^{137}Cs in the coastal region off Japan, we tracked ^{137}Cs in two types of flow fields: one from Global-FVCOM with a horizontal resolution of 2 km along the coast around the FNPP and the other from the nested JC-FVCOM-Global-FVCOM system with a resolution of 5 m in and around the FNPP. The first set of experiments used the same approach as previous studies (Kawamura et al., 2011; Tsumune et al., 2012; and Estournel et al., 2012), in which the ^{137}Cs discharge was treated as a point source at the coast in a regional model, while the second set of experiments had sufficient resolution to simulate the ^{137}Cs discharge from the FNPP through the different pathways into the ocean.

We adopted a similar approach as used by Tsumune et al. (2012) and Estournel et al. (2012) to determine inversely the amount of ^{137}Cs at the source based on the best fit with observations made at the northern discharge canal (1F-N) and the southern discharge canal (1F-S) of FNPP (Fig. 2). The model-predicted ^{137}Cs field was validated with comparisons to the monitored concentrations at 2F and Iwasawa south of 1F-S and other TEPCO, MEXT and WHOI measurements data made in the near-shore and offshore regions.

In this study, direct atmospheric loading was not considered. As reported by Kawamura et al. (2011) and Tsumune et al. (2012), almost all of the ^{137}Cs atmospheric deposition into the ocean occurred in March, with very little later. While atmospheric loading can be easily included in a tracer model, an accurate estimate of the time- and spatial-dependent ^{137}Cs loading that occurred during March was not available, so previous modeling assessments were focused solely on the direct water discharge at the coast. We followed the same strategy in our tracer experiments. To avoid underestimation due to the lack of atmospheric loading, we started tracking ^{137}Cs on March 26, 2011, with the understanding that the model-data mismatch in late March would likely be caused by atmospheric loading. Since the ^{137}Cs loading from leaking sources were adjusted by best fitting with measurements at sites 1F-N and 1F-S at the two canal exits, the model simulation should indirectly account for some of the actual atmospheric deposition occurring in late March. Our focus here is to examine the importance of resolving the complex structure of the FNPP on predicting the initial spread of ^{137}Cs in the Japanese coastal region. This approach could help us separate the impacts of the water source on the oceanic environment from the atmospheric source.

3 Results

3.1 Comparisons with observations

The results of the high-resolution model case predicted by the nested JC-FVCOM/Global-FVCOM will be presented first, followed by a comparison with the Global-FVCOM coarse-resolution model case.

The ^{137}Cs released at the nuclear reactor sites within the FNPP facility flowed out of the FNPP mainly through the channel bounded by the northern and southern breakwaters (Fig. 2; Ohnishi, 2012). In our high-resolution model case, which direction and how much ^{137}Cs flowed to the 1F-N and 1F-S site outside the breakwaters depended on whether or not the model was capable of resolving the local water flushing processes around FNPP. The observed ^{137}Cs concentration at these two sites varied with the same trend but slightly difference amplitudes, reached two peaks around the end of March and early April, and then rapidly decayed with time after April 12, 2011 (Fig. 5). By tuning the amount of ^{137}Cs at the source, the high-resolution model reproduced these variations reasonably well. This suggested that the model could provide a realistic flow exchange process between FNPP and the adjacent ocean.

Sites 2F and Iwasawa are located near the coast about 9 and 14 km south of 1F-S, respectively. The model-data comparison at these two sites again captured the observed rapid increase in ^{137}Cs concentration in late March and the gradual decay trend in April (Fig. 6). But, at these sites the peak concentration of ^{137}Cs was about 1~2 orders of magnitude smaller than that at 1F-S.

A further comparison was made at eight MEXT sites over the shelf (Fig. 7). The measurements suggest that, excluding atmospheric loading, a significant amount of ^{137}Cs in the radioactive water from the FNPP arrived in this shelf area about two weeks after leaking started. Although the MEXT sites were only about 30 km away from the coast, the maximum ^{137}Cs concentrations were about 10^2-10^3 lower compared with the peak values observed at the monitoring site 1F-S. The ^{137}Cs concentrations at MEXT sites reached a peak value of ~ 100 Bq/L at the end of April and then rapidly decreased to ~10 Bq/L or less during May. The model-computed ^{137}Cs concentration and its decay trend with time were in reasonable agreement with observations. For example, at site MEXT-3, the observed ^{137}Cs concentration was slightly lower than 100 Bq/L in early April and lower than 10 Bq/L in early June. These two values and varying trends were well captured by the model. For the given same time, the model suggested that the ^{137}Cs concentrations were higher at the northern sites than at the southern sites. It is thought that the ^{137}Cs detected at the MEXT sites before April 8 was due to atmospheric deposition (Kawamura et al., 2011; Estournel et al., 2012; Tsumune et al. 2012). Since neither atmospheric deposition nor an initial field of ^{137}Cs concentration was set up in the current study, no direct comparison with observational value recorded during that period should be made.

We next compared the model-computed ^{137}Cs concentrations with observed data at the same location and time where measurements were made for all available data sources, including TEPCO, MEXT, and WHOI. At the surface (Fig. 8), starting in early April, the model-computed ^{137}Cs concentration matched well with MEXT and TEPCO measurements. A mismatch appeared in late March that was likely a result of atmospheric deposition, which is omitted in our study. TEPCO measurement sites were located in the near-shore regions close to FNPP. Good agreement between model-computed and observed ^{137}Cs concentrations for TEPCO data in April through August suggests that the high-resolution model succeeded in resolving the advection and dispersion processes near the coast. A good match was also found for MEXT data from April to May, indicating that the model was also robust to capture these physical processes in the inner shelf region over a time scale of a month after leaking started. The model, however, tended to overestimate the ^{137}Cs concentrations recorded during the WHOI June survey and at MEXT sites in August. The WHOI survey started with one transect roughly around the 200-m isobath 30 km from the coast followed by other transects across the slope and eastward Kuroshio main stream. Placing both model-computed and observed ^{137}Cs concentrations at measurement sites and creating images based on these data (Fig. 9), we can see that the model was robust in predicting the spatial distribution of ^{137}Cs concentration that were observed during the WHOI June survey, but it tended to overestimate the size of the ^{137}Cs concentration plume and its values in the mid-shelf and slope regions.

Near the bottom (Fig. 10), however, the model-computed ^{137}Cs concentration was generally lower than the observed values at both TEPCO and MEXT monitoring sites. The overestimation at the surface and underestimation near the bottom implies that in addition to vertical diffusion and mixing, there were other physical processes that were responsible for a downward flux of ^{137}Cs in the water column. By adding a sinking term in the ^{137}Cs tracer model, one should be able to improve the simulation results. The critical issue is that such a sinking term is related to sedimentation over the shelf with the sinking velocity varying significantly with different types of sediment. We will discuss this issue in the next section.

3.2 Comparisons between high- and coarse-resolution models

The ^{137}Cs was mainly transported into the Japan's coastal shelf through a pumping-like process from the narrow exit between the FNPP northern and southern breakwaters. As a result of tidal flushing and dumping of cooling water into FNPP, the maximum outflow at the exit was about ~ 2 m/s. This strong outflow was jet-like and formed a cyclonic vortex initially due to shear instability (Fig. 11). With a continuous supply of water from the exit, this vortex became large and then separated into several large cyclonic and anticyclonic vortexes in late March before entering the continental shelf where the regional-scale circulation became dominant. Once the ^{137}Cs tracer was over the shelf where the water depth was 50-100 m or deeper, its spread was strongly influenced by the local wind and regional circulation (Fig. 12). In April, the tracer appeared like a coastal plume, which moved forth and back in the south-north direction along the coast. In May, the ^{137}Cs plume was still constrained within the coastal region but had a significant southward transport. It arrived in the southern region about 180 km south of FNPP in mid-May, where a portion of the ^{137}Cs was carried offshore by the eastward-flowing Kuroshio. At the same time, the northward wind caused coastal upwelling and wind-induced Ekman flow advected and dispersed the ^{137}Cs plume offshore. In July and August, the plume was predominantly transported towards the north and gradually dispersed into the interior of the Pacific Ocean. These results are consistent with the ^{137}Cs samples collected at Hasaki - a coastal station 180 km south of FNPP by Aoyama et al. (2012) and measurements made at ten sites along the northern coast of Sanriku and Tsugaru Strait north of FNPP by Inoue et al. (2012).

To our knowledge, all previous model assessments of the ^{137}Cs spreading were made with a regional-scale model without resolving the geometry of FNPP. Key questions here are: is the initial pumping process from FNPP critical for a model to produce a realistic spread of ^{137}Cs from the FNPP, or could the near-shore process be ignored if one is only interested to predict the ^{137}Cs spread over a regional scale? To address these questions, we followed the methods used in previous model assessments and tracked ^{137}Cs in the flow field predicted by Global-FVCOM.

In this regional model case, because the 2-km resolution grid was unable to resolve the FNPP facility and breakwater complex, the leaking ^{137}Cs was treated as a point source with the same rate of release used in the high-resolution model. The resulting spread of ^{137}Cs predicted by Global-FVCOM differed significantly from the high-resolution model case. At 4:00 GMT March 26, for example, the high-resolution nested model showed that the ^{137}Cs tracer was still around the FNPP exit, but the Global-FVCOM-computed ^{137}Cs concentration was distributed symmetrically in relation to the point source and covered a much larger area with a width of ~ 0.2° in latitude along the coast (Fig. 12: upper panels). At 00:00 GMT June 1, the ^{137}Cs concentration predicted by Global-FVCOM had spread in the entire shelf and slope region up to 43°N, while the ^{137}Cs concentration computed by the high-resolution nested model remained high near the coast and no tracer was found north of 41°N (Fig. 12: lower panels). It is clear that Global-FVCOM significantly overestimated the size of the plume. As a result, the model-computed ^{137}Cs concentrations were significantly lower than observations at both near-shore and offshore measurement sites (Fig. 13).

The high- and coarse-resolution model results can help us understand why previous modeling efforts failed to reproduce the temporal variation of the ^{137}Cs concentration over the shelf region. Applying a 2-km resolution Regional Ocean Model System (ROMs) to the Japanese coast, Tsumune et al. (2012) conducted a tracer experiment to predict the ^{137}Cs spread over the shelf. The model did capture the ^{137}Cs concentration peak at MEXT-8 in mid-April, but significantly underestimated ^{137}Cs concentrations at the other MEXT-1 to MEXT-7 sites. Coincidentally, Estournel et al. (2012) reported that their model also underestimated ^{137}Cs concentrations at all MEXT sites, even though they increased the grid resolution to 600 m. They attributed this underestimation to the lack of information on the river discharge in the model which could cause a thin, low-salinity surface layer and enhance the offshore transport under the influence of wind. Our results, however, suggest that in order to reproduce the observed spread of ^{137}Cs over the shelf, a model needs to resolve the realistic coastal geometry of the FNPP and adjacent region. In order to reproduce the dispersion process from the leaking source to 1F-N and 1F-S, a model must be capable of resolving the complex small-scale vortex current field that controlled the water exchange or pumping around FNPP. Failure to capture this initial pumping process could lead to the unrealistic ^{137}Cs spreading over the shelf.

As we pointed out in the introduction, the spread of ^{137}Cs is controlled mainly by advection and dispersion processes. Chen et al. (2008) derived analytically the governing equations controlling the movement of the center of a small-scale dye patch in the coastal ocean. The equations indicate that after the dye is released, the movement of the dye patch is driven by the ensemble velocity integrated through the dye patch and the concentration flux related to the vertical shear of the horizontal velocity of the dye patch. Considering a dye patch that moves conservatively in the ocean, the total amount of the dye remains unchanged, but its concentration can change significantly as a result of deformation of the dye patch due to vertical and lateral dispersion that are related to velocity shears and turbulent diffusion. In order to capture the dye spreading, it is critical to resolve the realistic vertical and lateral diffusion processes. For many coastal ocean models, the horizontal diffusion is parameterized using a Smagorinsky eddy parameterization method (Smagorinsky, 1963), which depends on the model resolution and velocity shears.

Our results indicate that an underestimation of ^{137}Cs concentration over the shelf predicted by Global-FVCOM was mainly due to the overestimation of ^{137}Cs spreading in the coastal region. This overestimation was caused by insufficient grid resolution to capture realistic lateral diffusion. This explanation can be applied to previous regional model simulations and emphasize the critical importance of model resolution in the parameterization of lateral diffusion.

4 Discussion

Like previous modeling efforts, we treated ^{137}Cs as a dissolved conservative tracer without including flocculation processes to suspended sediments. The overestimation at the surface and underestimation near the bottom in the model-predicted ^{137}Cs concentration implies that sedimentation processes should be included if one attempts to make an accurate prediction of the spread of ^{137}Cs over the shelf. This finding was also anticipated by Estournel et al. (2012) who suggested that an overestimation of the predicted ^{137}Cs concentration can probably be caused by ignoring a sinking term in the tracer equation. The suggestions from these modeling experiments are supported by the ^{137}Cs concentration levels found in the bottom sediment layer at monitoring sites along the Japanese coast. At many monitoring sites in the shelf region between the 50-m and 200-m isobaths, the observed ^{137}Cs concentration in sediments increased significant with time (Fig. 14). In monitoring sites around FNPP, the sediment ^{137}Cs concentrations showed high values before July and then decreased rapidly with time afterward (Fig. 15). A simple estimation indicates that during April-June, the model-data discrepancy values at the surface and near the bottom were about 48% and -39% in the coastal area. So, without adding a sinking term in the ^{137}Cs tracer equation, about 9% more of the total amount of ^{137}Cs remained in the seawater than what was measured. Assuming these extra amounts were deposited in the sediment through sedimentation, this means that at least 9% of the discharged ^{137}Cs was removed by sedimentation. The rapid drop in ^{137}Cs

concentrations at monitoring sites in the coastal region around FNPP after July implies that the ^{137}Cs in sediment layers could be re-suspended and carried offshore through advection and mixing processes. This can be inferred since the observation data showed that the concentration of radioactive materials through the end of July remained higher than expected in the coastal region (Buesseler et al., 2011). Because these processes varied significantly in space and time and the lack of knowledge about the ^{137}Cs-sediment flocculation processes, it was not feasible to attempt to include sedimentation in our ^{137}Cs tracking experiments.

5 Summary

A high-resolution global-coastal nested ocean model was developed to simulate the initial spreading of ^{137}Cs over the Japan shelf after the March 11, 2011 Fukushima Dai-ichi Nuclear Power Plant failure. With sufficient resolution to resolve the complex water exchange process between the FNPP and adjacent coastal ocean, this nested model succeeded in reproducing the temporal variation and spatial distribution of ^{137}Cs over the shelf during the April-August period. The comparison between high-resolution nested and regional-scale models clearly showed that given the same discharge of ^{137}Cs, the model-predicted spreading of ^{137}Cs was sensitive not only to model resolution but also geometric fitting. Failure to capture this initial dispersion process from the leaking source to the 1F-N and 1F-S monitoring sites could lead to an unrealistic prediction of ^{137}Cs spreading over the shelf. A coarse-resolution (~2 km) regional scale model overestimated lateral diffusion and thus caused faster dispersion of ^{137}Cs from the coast to the deep ocean.

The ^{137}Cs spreading process predicted by the high-resolution nested model was in good agreement with measurements over the inner shelf, but showed an overestimation at the surface and underestimation near the bottom in the offshore region. These model-data discrepancies were mainly due to the assumption that treated ^{137}Cs as a dissolved conservative tracer without inclusion of flocculation processes to suspended sediments. The importance of sedimentation was evident in both model results and ^{137}Cs measurements made in the bottom sediment at monitoring sites in the coastal region.

Acknowledgements

We would like to thank K. Buesseler and S. Jayne at WHOI who kindly shared their research results and June 2011 survey data with us. This project was supported by the US National Science Foundation RAPID grants #1141697 and #1141785 and the Japan Science and Technology Agency J-RAPID program. The development of Global-FVCOM was supported by NSF grants ARC0712903, ARC0732084, and ARC0804029. Z. Lai's contribution was also supported by the Natural Science Foundation of China project 41206005, China MOST project 2012CB956004, and Sun Yat-Sen University 985 grant 42000-3281301. C. Chen serves as chief scientist for the International Center for Marine Studies, Shanghai Ocean University, and his contribution was supported by the Program of Science and Technology Commission of Shanghai Municipality (09320503700).

References

Aoyama, M., Tsumune, D., Uematsu, M., Kondo, F. and Hamajima, Y.: Temporal variation of ^{134}Cs and ^{137}Cs activities in surface water at stations along the coastline near the Fukushima Dai-ichi Nuclear Power Plant accident site, Japan, Geochemical Journal, 46, 321-325, 2012.

Beardsley, R.C., C. Chen, Z. Lai, J. Sasaki, H. Lin, J. Lin, and R. Ji (2012), US-Japan Collaborative Research on the March 11, 2011 Earthquake, Tsunami Inundation, and Initial Spread of Fukushima Radionuclides into the Pacific Ocean, 2012 Ocean Sciences Meeting (poster).

Behrens, E., Schwarzkopf, F.U., Lübbecke, J.F., and Böning, C.W.: Model simulations on the long-term dispersal of ^{137}Cs released into the Pacific Ocean off Fukushima, Environmental Research Letters, 7, 034004, doi:10.1088/1748-9326/7/3/034004.

Buesseler, K., Aoyama, M., and Fukasawa, M.: Impacts of the Fukushima Nuclear Power Plants on Marine Radioactivity, Environmental Science & Technology, 45, 9931-9935, 2011.

Chen, C., Liu, H. and Beardsley, R.: An unstructured grid, finite-volume, three dimensional, primitive equations ocean model: Application to coastal ocean and estuaries, Journal of Atmospheric & Ocean Technology, 20 (1), 159–186, 2003.

Chen, C, Beardsley, R.C. and Cowles, G.: An unstructured grid, finite-volume coastal ocean model (FVCOM) system, Special Issue entitled “Advances in Computational Oceanography”, Oceanography, 19(1), 78-89, 2006a.

Chen, C., Cowles, G. and Beardsley, R.C.: An unstructured grid, finite-volume coastal ocean model: FVCOM User Manual, Second Edition, SMAST/UMASSD Technical Report-06-0602, pp 315, 2006b.

Chen, C., Huang, H., Beardsley, R.C., Liu, H., Xu, Q., and Cowles, G.: A finite-volume numerical approach for coastal ocean circulation studies: comparisons with finite difference models. J. Geophys. Res. 112, C03018, doi:10.1029/2006JC003485, 2007.

Chen, C., Xu, Q., Houghton, R., and Beardsley, R.C.: A model-dye comparison experiment in the tidal mixing front zone on the southern flank of Georges Bank, Journal of Geophysical Research, 113, C02005, doi:10.1029/2007JC004106, 2008.

Chen, C., Z. Lai, R.C. Beardsley, H. Lin, J. Sasaki, J. Lin, and R. Ji (2012), Model Assessment of Inundation at the Fukushima Dai Nuclear Power Plant Facility and Initial Spread of Radionuclides in the Coast Ocean, 2012 Ocean Sciences Meeting (abstract).

Chen, C., Lai, Z., Beardsley, R.C., Sasaki, J., Lin, J., Lin, H. and Ji, R.: The March 11, 2011 Tōhoku M9.0 Earthquake-induced Tsunami and Coastal Inundation along the Japanese Coast: A Model Assessment, Journal of Geophysical Research, submitted.

Dietze, H. and Kriest, I.: ^{137}Cs off Fukushima Dai-ichi, Japan – model based estimates of dilution and fate, Ocean Science, 8, 319-332, 2012.

Estournel, C., Bosc, E., Bocquet, M., Ulses, C., Marsaleix, P., Winiarek, V., Osvath, I., Nguyen, C., Duhaut, T., Lyard, F., Michaud, H. and Auchair, F.: Assessment of the amount of cesium-137 released into the Pacific Ocean after the Fukushima accident and analysis of its dispersion in Japanese coastal waters, Journal of Geophysical Research, 117, C11014, doi:10.1029/2012JC007933, 2012.

Gao, G., C. Chen, J. Qi and R.C. Beardsley: An unstructured-grid, finite-volume sea ice model: development, validation and application. J. Geophys. Res., 116, C00D04, doi: 10.1029/2010JC006688, 2011.

Grossman, E.: Radioactivity in the Ocean: Diluted, But Far from Harmless, online: http://e360.yale.edu/feature/radioactivity_in_the_ocean_diluted_but_far_from_harmless/2391/.

Honda, M.C.H., Aono, T., Aoyama, M., Hamajima Y., Kawakami, H., Kitamura M., Masumoto Y., Miyazawa Y., Takigawa M., and Saino, T: Dispersion of artificial caesium-134 and -137 in the western North Pacific one month after the Fukushima accident, Geochemical Journal, 46, 1-9, 2012.

Hu, S.., C. Chen, R. Ji, D.W. Townsend, R. Tian, R.C. Beardsley and C.S. Davis: Effects of surface forcing on interannual variability of the fall phytoplankton bloom in the Gulf of Maine revealed using a process-oriented model. Mar. Ecol. Prog. Ser., 427, 29-49, doi: 10.3354/meps0904, 2011.

Inoue, M., Kofuji, H., Hamajima, Y., Nagao, S., K. Yoshida and Yamamoto, M.: ^{134}Cs and ^{137}Cs activities in coastal seawater along Northern Sanriku and Tsugaru Strait, northeastern Japan, after Fukushima Dai-ichi Nuclear Power Plant accident, Journal of Environmental Radioactivity, 111, 116-119, 2012.

Kawamura, H., Kobayashi, T., Furuno, A., In, T., Ishikawa, Y., Nakayama, T., Shima, S. and Awaji T.: Preliminary Numerical Experiments on Oceanic Dispersion of ^{131}I and ^{137}Cs Discharged into the Ocean because of the Fukushima Daiichi Nuclear Power Plant Disaster, Journal of nuclear science and technology, 48, 11, 1349-1356, 2011.

Lai, Z., C. Chen, R.C. Beardsley, H. Lin, J. Sasaki, and J. Lin (2012), Model Assessment of 2011 Japan Tsunami and Coastal Inundation Processes, 2012 Ocean Sciences Meeting (poster).

Ohnishi, T.: The Disaster at Japan's Fukushima-Daiichi Nuclear Power Plant after the March 11, 2011 Earthquake and Tsunami, and the Resulting Spread of Radioisotope Contamination, Radiation Research, 177, 1-14, 2012.

Oura, Y. and Ebihara, M.: Radioactivity concentrations of ^{131}I, ^{134}Cs and ^{137}Cs in river water in the Greater Tokyo Metropolitan area after the Fukushima Daiichi Nuclear Power Plant Accident, Geochemical Journal, 46, 303-309, 2012.

Smagorinsky, J.: General circulation experiments with the primitive equations, I. The basic experiment, Mon. Wea. Rev., 91, 99–164, 1963.

Tsumune, D., Tsubono, T., Aoyama, M. and Hirose, K.: Distribution of oceanic ^{137}Cs from the Fukushima Daiichi Nuclear Power Plant simulated numerically by a regional ocean model, Journal of Environmental Radioactivity, 111, 100-108, 2012.

Figure Captions

Figure 1. Schematic of the regional circulation pattern with an enlarged view of the Fukushima Daiichi Nuclear Power Plant.

Figure 2. Locations of the north discharge canal (1F-N) and the south discharge canal (1F-S), the 2F and Iwasawa stations at south of 1F-S and the eight MEXT sampling sites 30 km off the coast. The filled triangle indicates the location of the discharge source for leaking ^{137}Cs.

Figure 3. Location of MEXT, TEPCO and WHOI monitoring and survey measurement sites. Lower-left panel is an enlarged view of the near-shore monitoring sites bounded by a dashed line box.

Figure 4. A view of model grids for the global-Japan coastal nested FVCOM system used in this study. The Global-FVCOM grid covers the entire global ocean with a horizontal resolution of 2 km in the Japanese coastal region (shown in the right panel). The blue line in the right panel indicates the nesting boundary that link Global-FVCOM and the Japan coastal FVCOM (JC-FVCOM). The left panel is an enlarged view of JC-FVCOM.

Figure 5. Comparisons of model-computed and observed ^{137}Cs concentrations at 1F-N and 1F-S over the period March 26 to June 8, 2011.

Figure 6. Comparisons of model-computed and observed ^{137}Cs concentrations at 2F and Lwasawa over the period March 26 to June 8, 2011.

Figure 7. Comparisons of model-computed and observed ^{137}Cs concentrations at eight MEXT monitoring sites (30 km off the coast) for the period April 1 to June 8, 2011.

Figure 8. Logarithmic ratio of the high-resolution nested model-computed surface ^{137}Cs concentration to the observation at MEXT, TEPCO and WHOI measurement sites over the period March 26 to August 31, 2011.

Figure 9. Comparisons of high-resolution nested model-computed and observed (from the June WHOI survey) surface ^{137}Cs concentrations at the survey sites in June, 2011.

Figure 10. Logarithmic ratio of the model-computed ^{137}Cs bottom concentration to the observation at MEXT and TEPCO measurement sites over the period March 26 to August 31, 2011.

Figure 11. Distributions of the high-resolution nested model computed surface ^{137}Cs concentration around FNPP at 01:00, 02:00, 03:00 and 04:00 GMT, March 26, 2011. Label "C" indicates the location of a cyclonic vortex, and label "A" indicates the location of an anti-cyclonic vortex.

Figurer 12. Distributions of the high-resolution nested model computed surface ^{137}Cs concentration in the Japan's coastal region at 15:00 GMT April 15; 15:00 GMT May 15; 00:00 GMT July 1; and 00:00 GMT August 1, 2011.

Figure 13. Comparisons of distributions of the ^{137}Cs concentrations predicted by the nested Global-FVCOM and JC-FVCOM model (left panels) and the Global-FVCOM (right panels) at 04:00 GMT March 26 and 00:00 GMT June 1, 2011.

Figure 14. Logarithmic ratio of the Global-FVCOM-computed surface ^{137}Cs concentration to the observation at MEXT and TEPCO measurement sites during April and May, 2011.

Figure 15. Time series of the ^{137}Cs concentration (unit: Bq/kg) measured in sediments in the outer-shelf monitoring sites during April to October 2011.

Figure 16. Time series of the ^{137}Cs concentration (unit: Bq/kg) measured in sediments in the near-shore monitoring sites during June to December 2011.

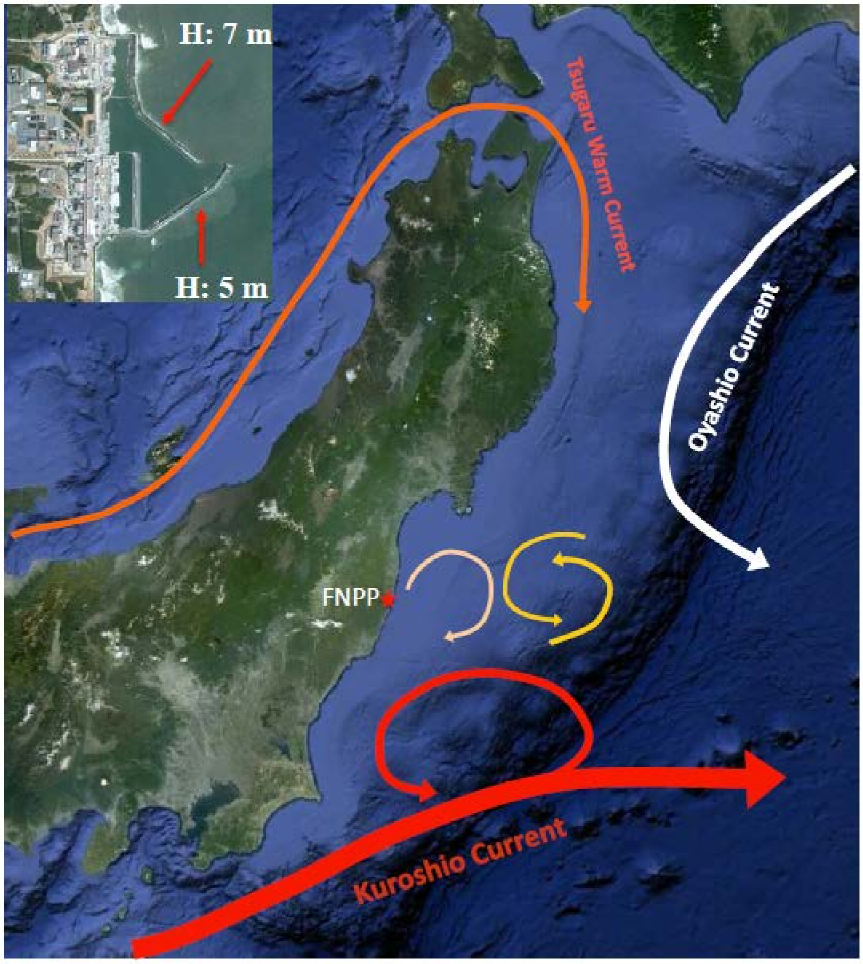
H: 7 m
H: 5 m
Tsugaru Warm Current
Oyashio Current
FNPP
Kuroshio Current

Fig. 1

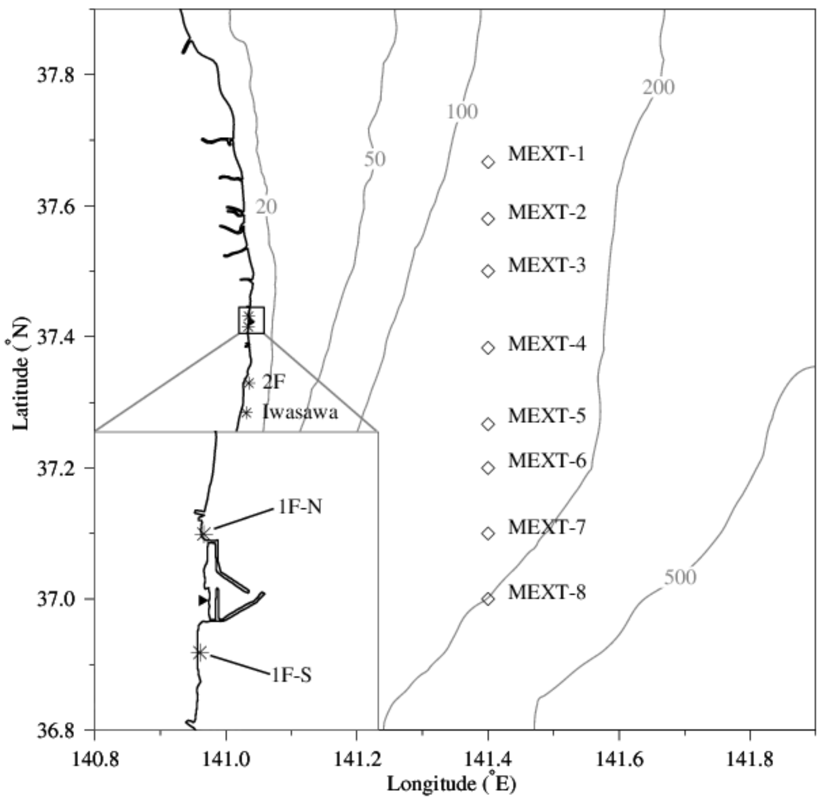

37.8
37.6
37.4
37.2
37.0
36.8
Latitude (°N)
140.8
141.0
141.2
141.4
141.6
141.8
Longitude (°E)
20
50
100
200
500
MEXT-1
MEXT-2
MEXT-3
MEXT-4
MEXT-5
MEXT-6
MEXT-7
MEXT-8
2F
Iwasawa
1F-N
1F-S

Fig. 2

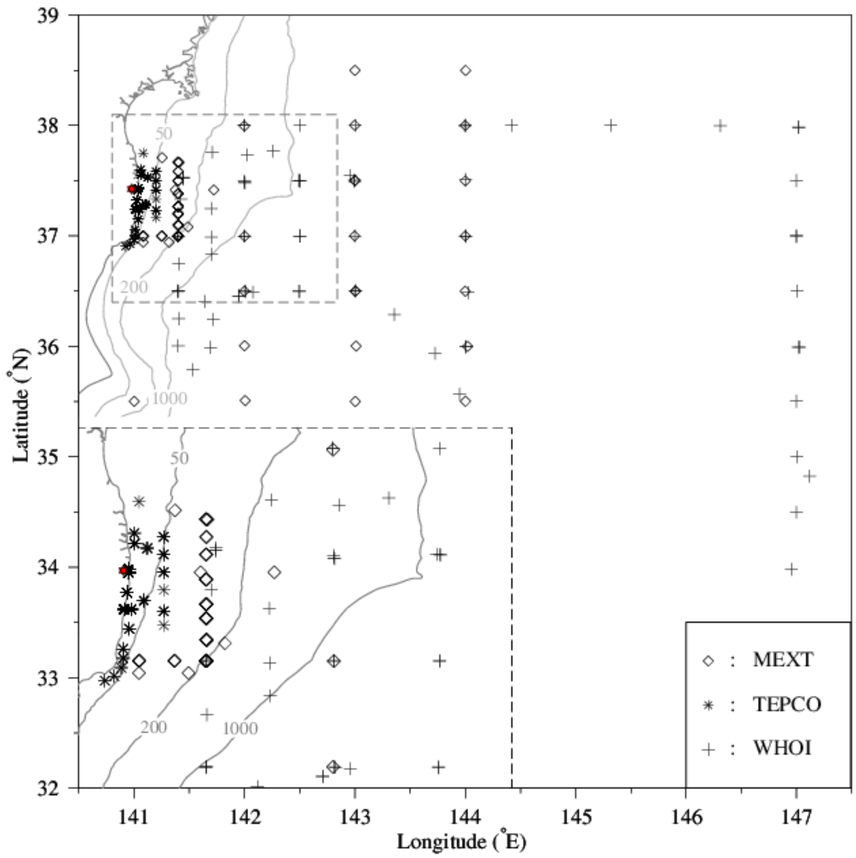

Latitude (°N)
Longitude (°E)
39
38
37
36
35
34
33
32
141
142
143
144
145
146
147
50
200
1000
50
200
1000
◇ : MEXT
* : TEPCO
+ : WHOI

Fig. 3

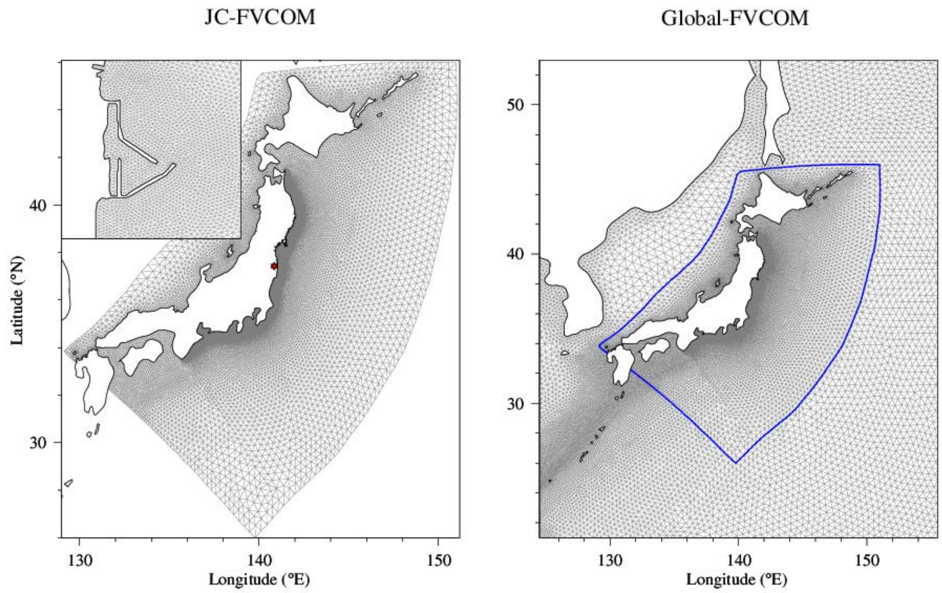
JC-FVCOM
Global-FVCOM
Latitude (°N)
Longitude (°E)
40
30
50
130
140
150

Fig. 4

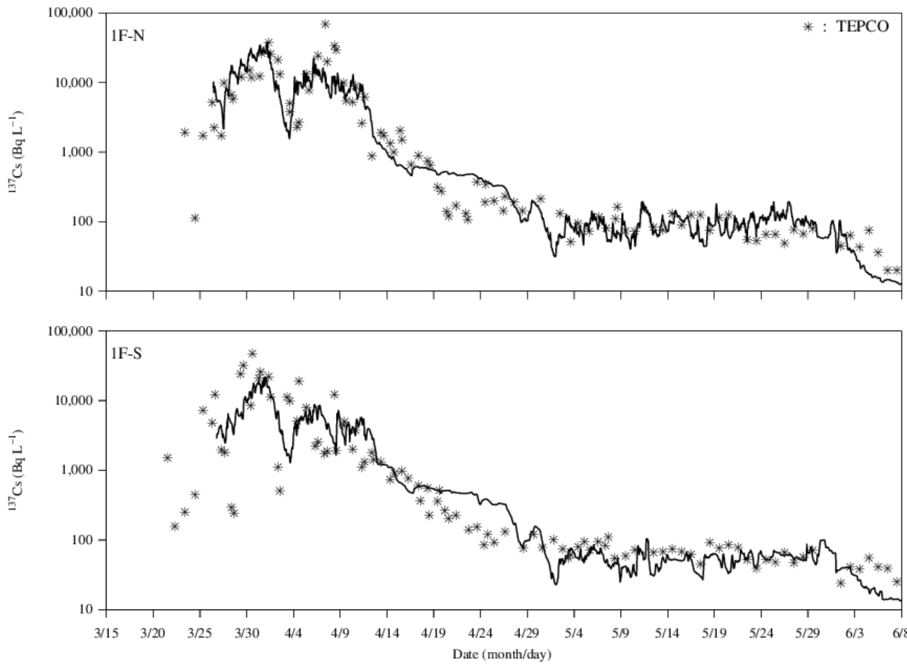
1F-N
∗ : TEPCO
1F-S
^{137}Cs (Bq L^{-1})
100,000
10,000
1,000
100
10
3/15
3/20
3/25
3/30
4/4
4/9
4/14
4/19
4/24
4/29
5/4
5/9
5/14
5/19
5/24
5/29
6/3
6/8
Date (month/day)

Fig. 5

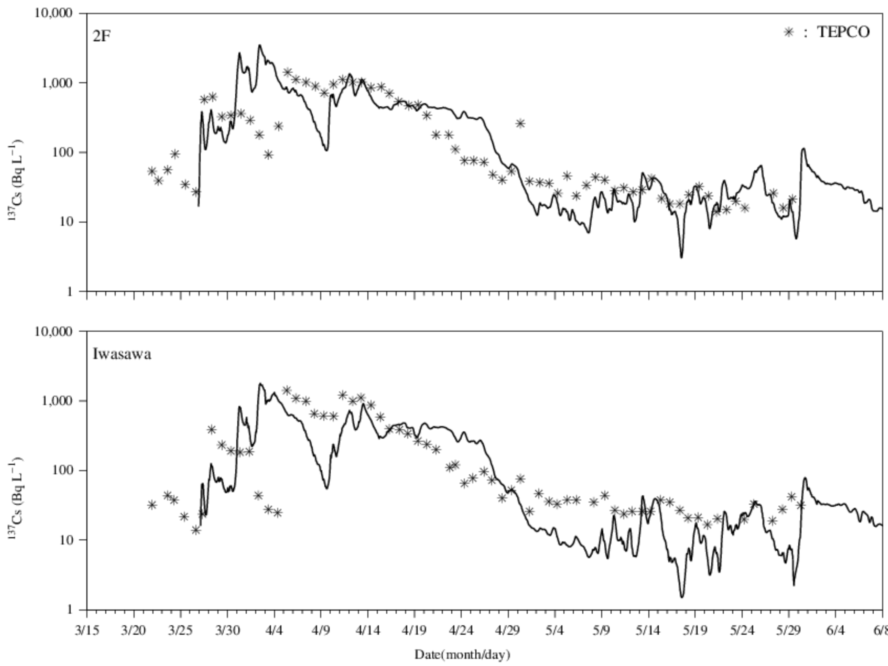
2F
＊ : TEPCO
Iwasawa
^{137}Cs (Bq L^{-1})
10,000
1,000
100
10
1
3/15
3/20
3/25
3/30
4/4
4/9
4/14
4/19
4/24
4/29
5/4
5/9
5/14
5/19
5/24
5/29
6/4
6/8
Date(month/day)

Fig. 6

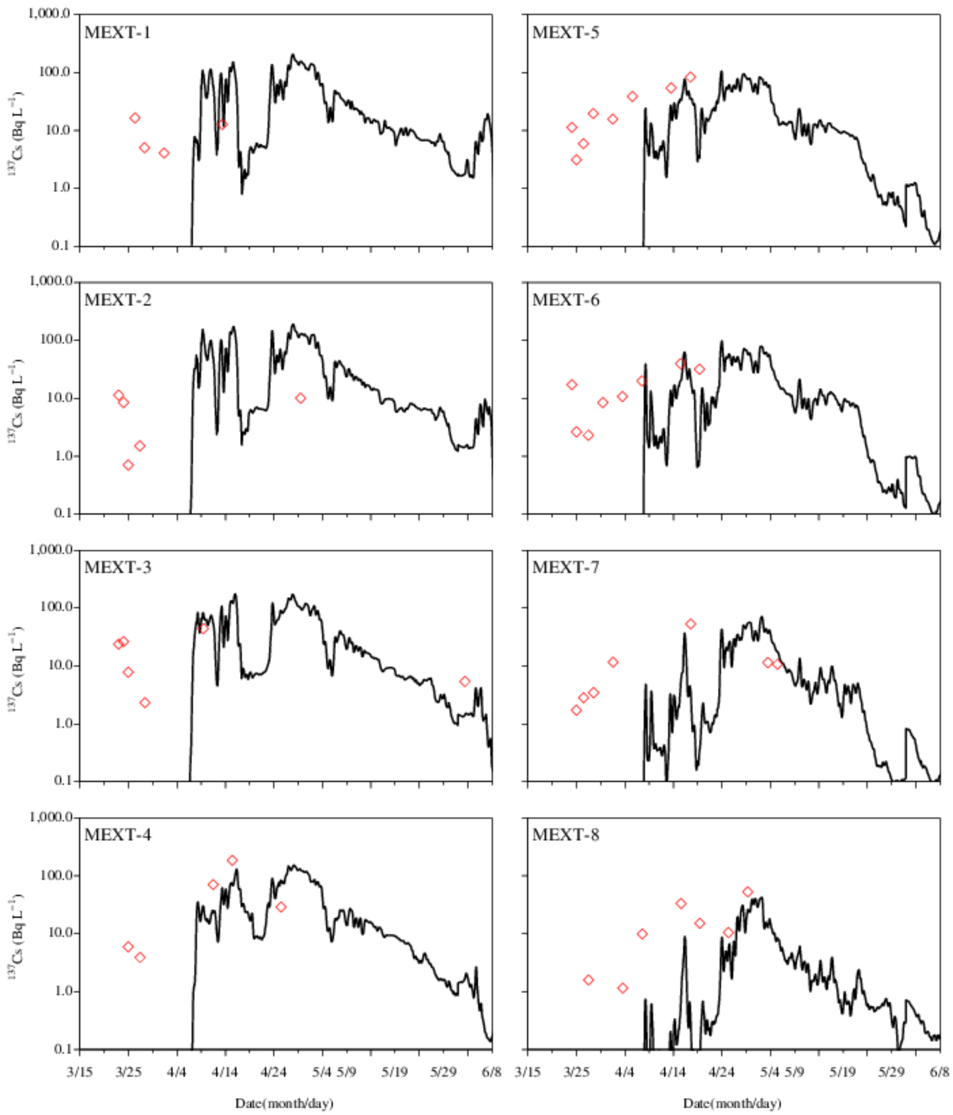
MEXT-1
MEXT-2
MEXT-3
MEXT-4
MEXT-5
MEXT-6
MEXT-7
MEXT-8
1,000.0
100.0
10.0
1.0
0.1
137Cs (Bq L−1)
3/15
3/25
4/4
4/14
4/24
5/4
5/9
5/19
5/29
6/8
Date(month/day)

Fig. 7

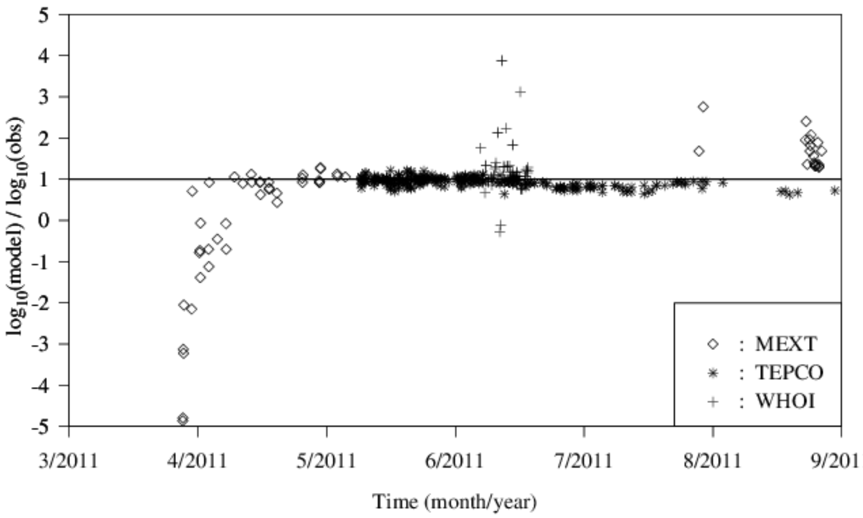

log10(model) / log10(obs)
5
4
3
2
1
0
-1
-2
-3
-4
-5
3/2011
4/2011
5/2011
6/2011
7/2011
8/2011
9/2011
Time (month/year)
◇ : MEXT
∗ : TEPCO
+ : WHOI

Fig. 8

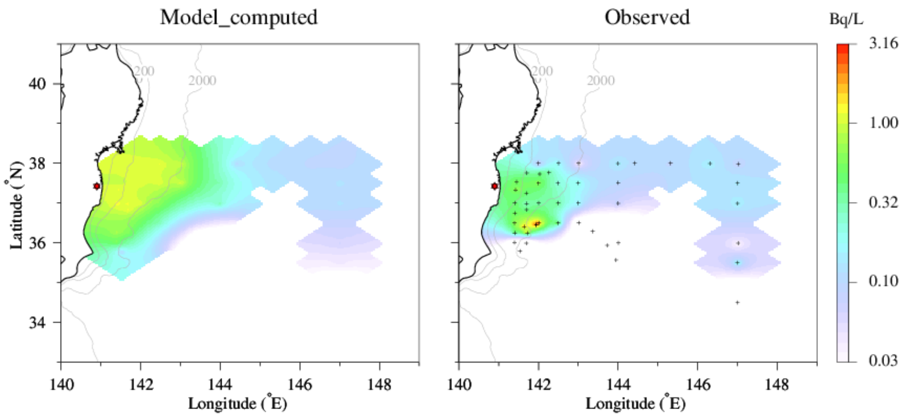
Model_computed
Observed
Bq/L
3.16
1.00
0.32
0.10
0.03
200
2000
Latitude (°N)
40
38
36
34
140
142
144
146
148
Longitude (°E)

Fig. 9

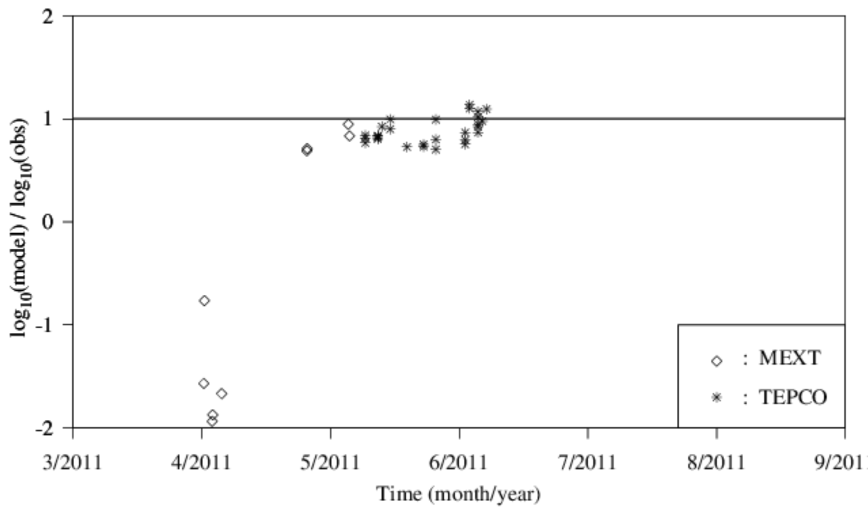

2
1
0
-1
-2
$\log_{10}$(model) / $\log_{10}$(obs)
3/2011
4/2011
5/2011
6/2011
7/2011
8/2011
9/2011
Time (month/year)
◇ : MEXT
* : TEPCO

Fig. 10

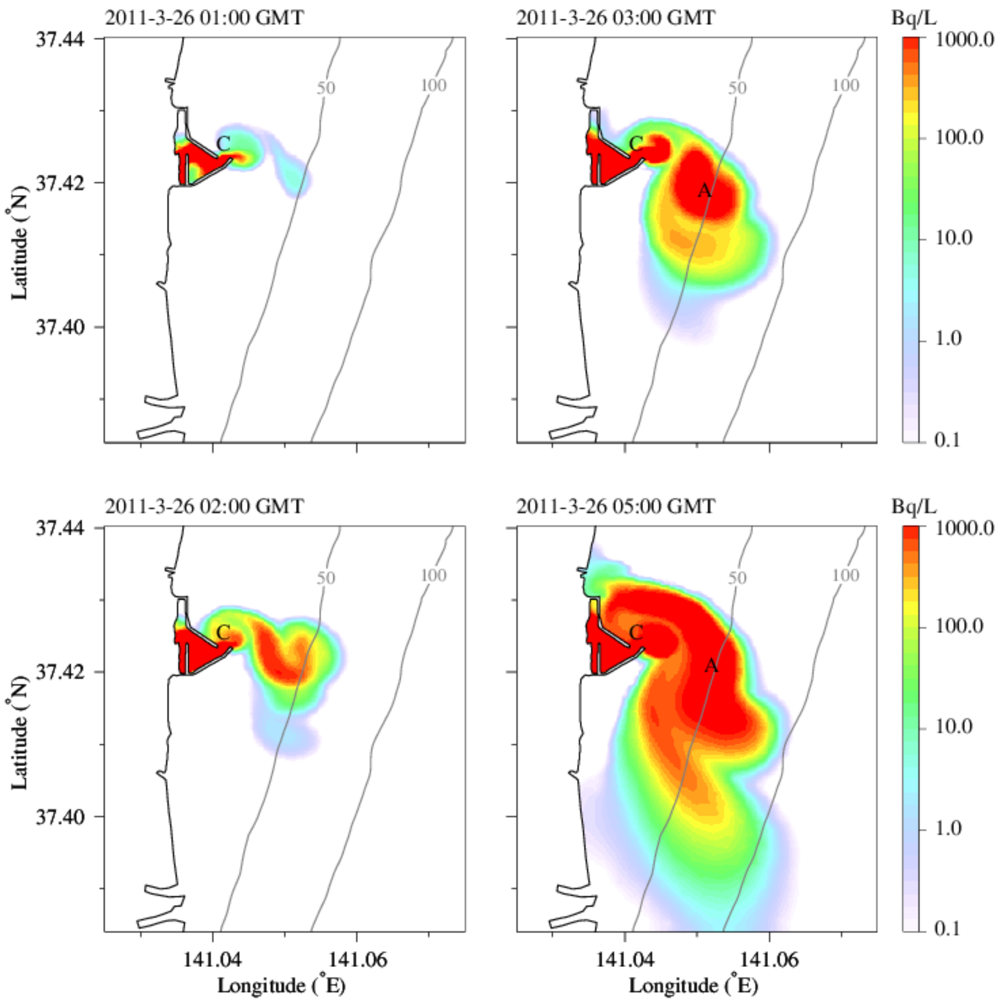
2011-3-26 01:00 GMT
2011-3-26 03:00 GMT
2011-3-26 02:00 GMT
2011-3-26 05:00 GMT
Bq/L
1000.0
100.0
10.0
1.0
0.1
37.44
37.42
37.40
Latitude (°N)
141.04
141.06
Longitude (°E)
50
100
C
A

Fig. 11

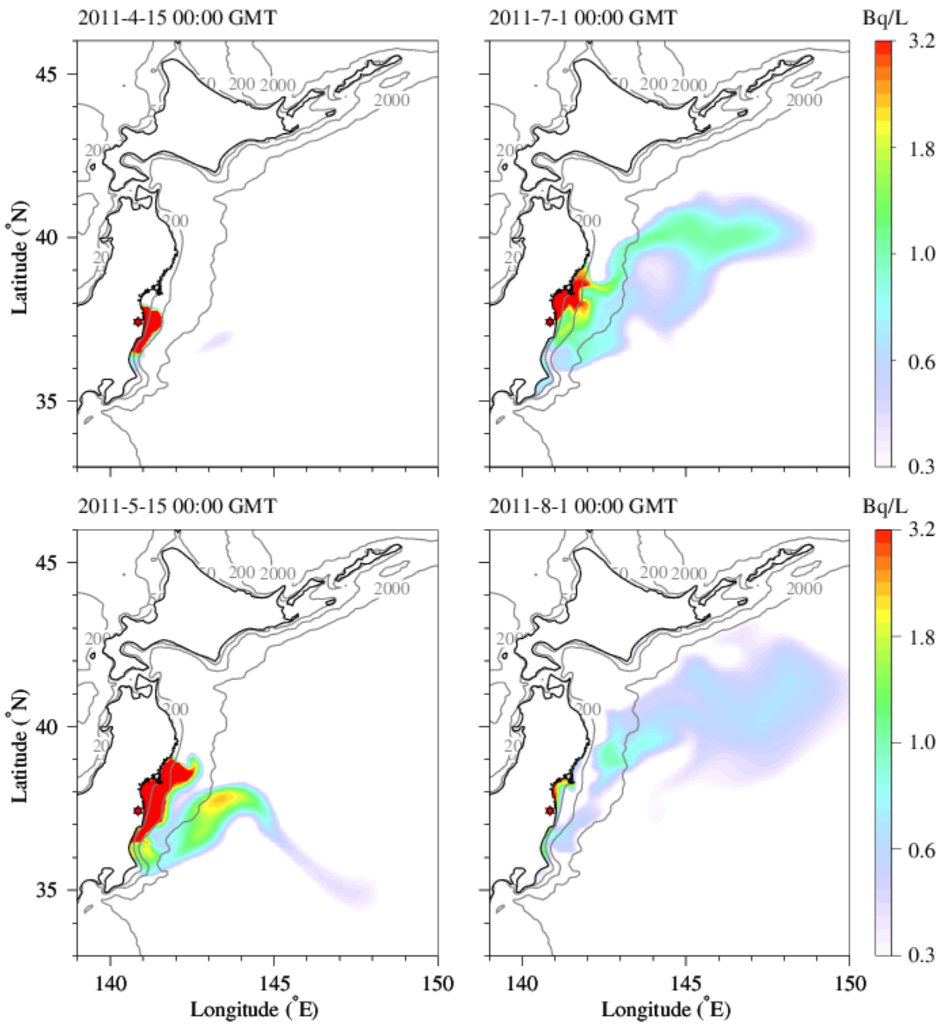
2011-4-15 00:00 GMT
2011-7-1 00:00 GMT
2011-5-15 00:00 GMT
2011-8-1 00:00 GMT
Bq/L
3.2
1.8
1.0
0.6
0.3
45
40
35
Latitude (°N)
140
145
150
Longitude (°E)
200
2000

Fig. 12

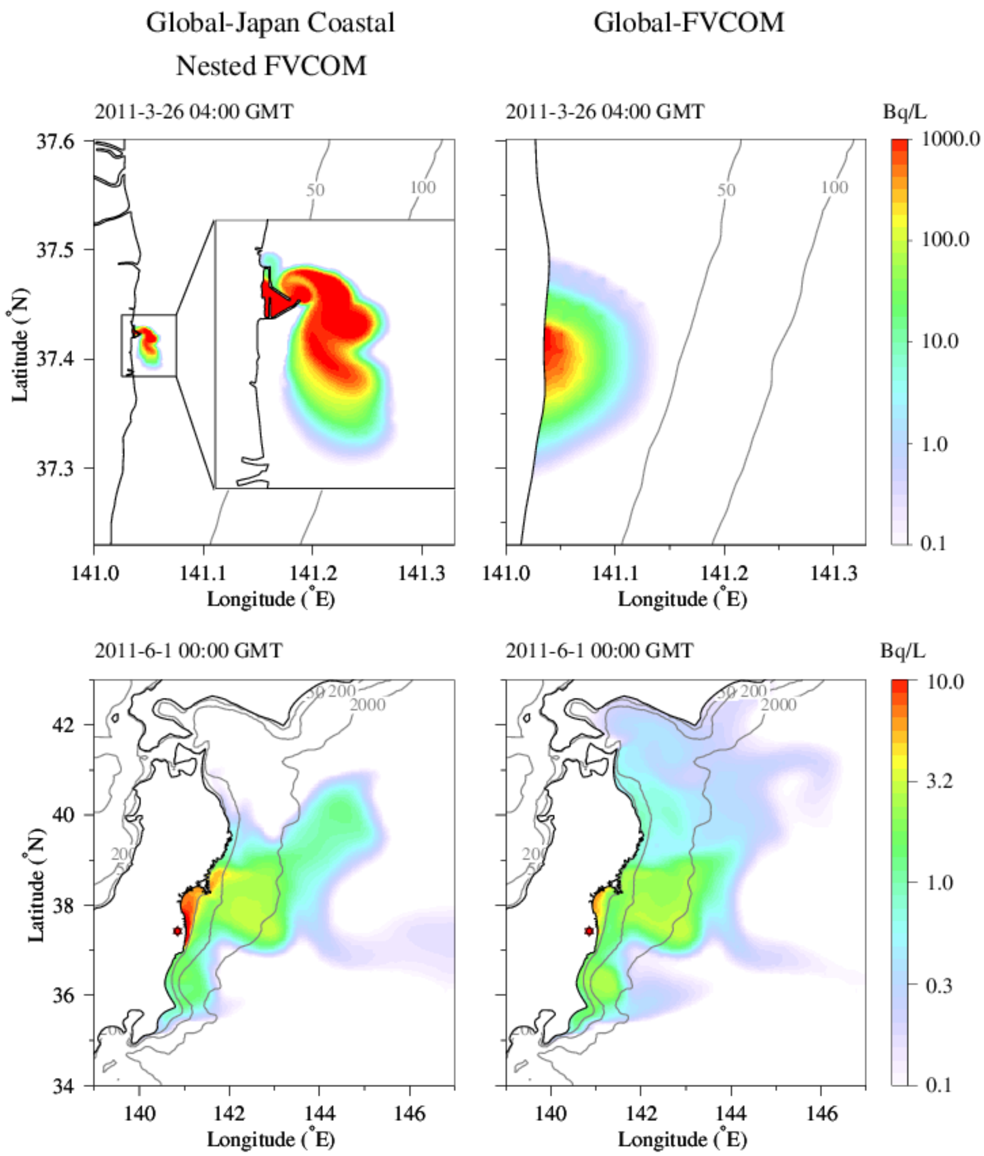
Global-Japan Coastal
Nested FVCOM
Global-FVCOM
2011-3-26 04:00 GMT
2011-3-26 04:00 GMT
Bq/L
1000.0
100.0
10.0
1.0
0.1
Latitude (°N)
Longitude (°E)
2011-6-1 00:00 GMT
2011-6-1 00:00 GMT
Bq/L
10.0
3.2
1.0
0.3
0.1
Latitude (°N)
Longitude (°E)

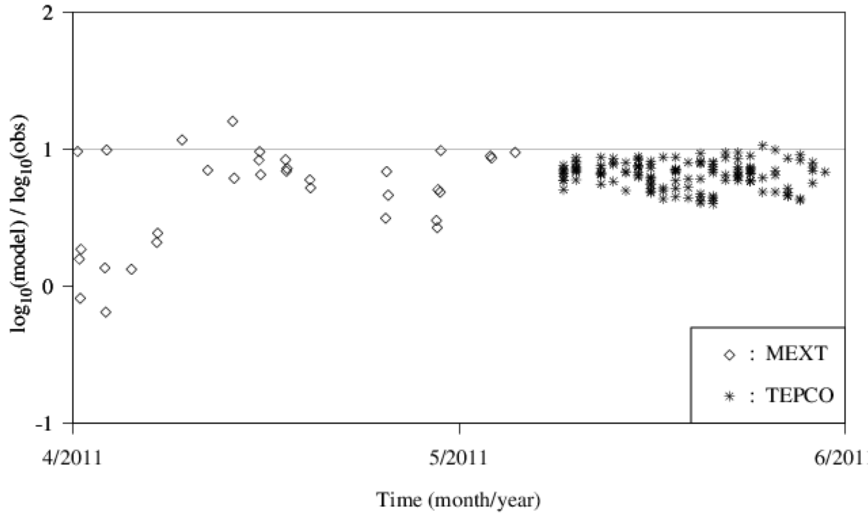

2
1
0
-1
log10(model) / log10(obs)
4/2011
5/2011
6/2011
Time (month/year)
◇ : MEXT
* : TEPCO

Fig. 14

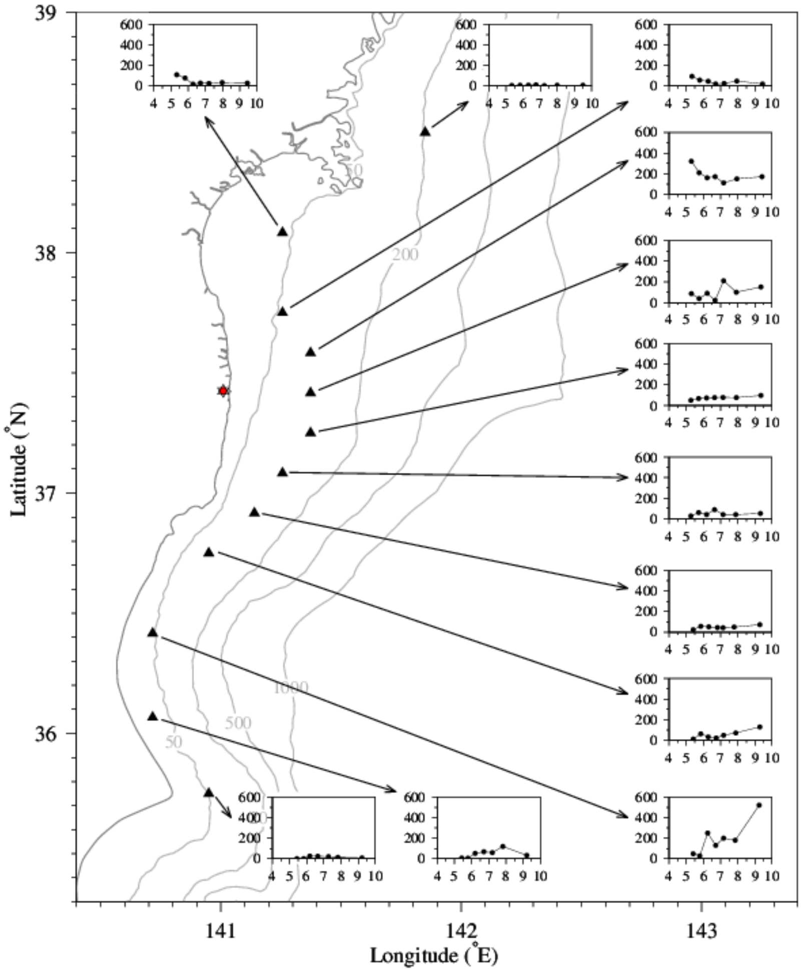

Fig. 15

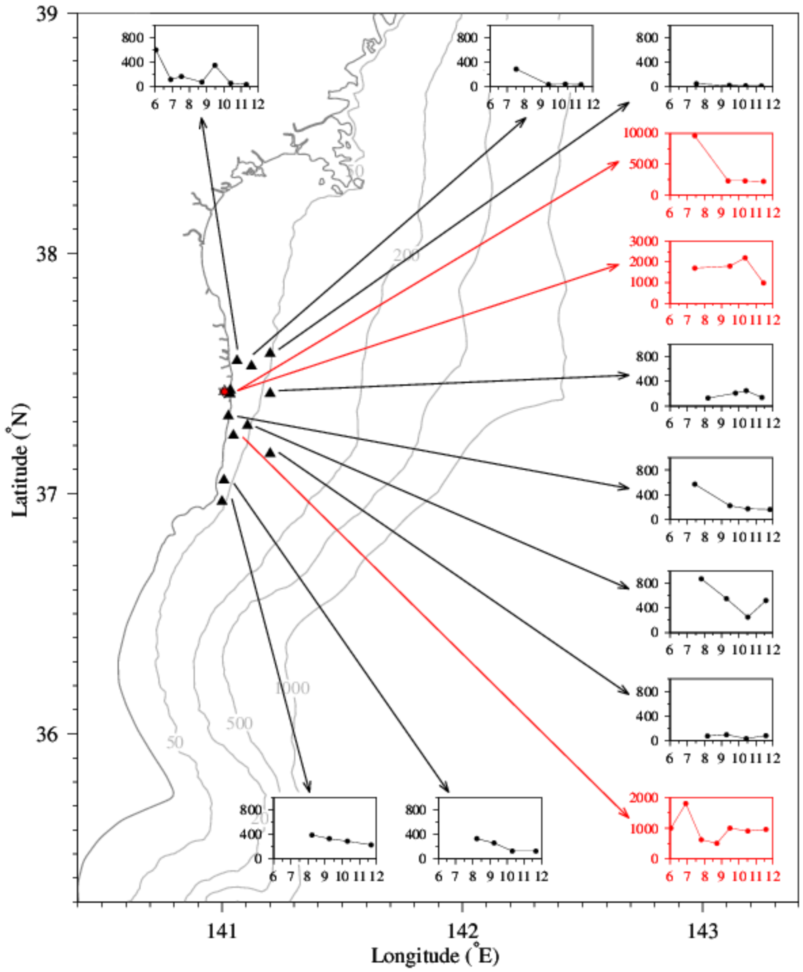

Fig. 16